

CONFIDENTIAL

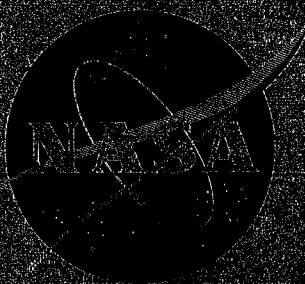
Copy

161

NASA TM

X-74

4-2-63



CASE FILE
COPY

TECHNICAL MEMORANDUM

X-74

STABILITY AND CONTROL CHARACTERISTICS
OF THE X-74 AIRPLANE

By Harold J. Walker and Chester H. Willowicz

Flight Research Center
Edwards, Calif.

NATIONAL AERONAUTICS AND SPACE ADMINISTRATION
WASHINGTON

March 1963

CONFIDENTIAL

NATIONAL AERONAUTICS AND SPACE ADMINISTRATION

TECHNICAL MEMORANDUM X-714

STABILITY AND CONTROL DERIVATIVE CHARACTERISTICS
OF THE X-15 AIRPLANE* **

By Harold J. Walker and Chester H. Wolowicz

SUMMARY

Flight measurements of the stability and control derivative characteristics have been made up to Mach numbers approaching the design limit (6.0) of the X-15 airplane and to angles of attack as high as 17° . These data are, with minor exceptions, in generally good agreement with the predictions from wind-tunnel tests and theory. No adverse longitudinal characteristics have been uncovered; however, an area of reduced lateral-directional stability and poor lateral-directional control has been observed at moderate angles of attack due to a positive trend in the dihedral derivative for Mach numbers above approximately 2.2.

INTRODUCTION


The need for reliable stability and control predictions is most urgent when the first flights of an advanced vehicle are attempted in new and unfamiliar areas, as in the current X-15 program. In planning such flights a complete compilation of the derivative characteristics is, of course, essential. Although wind-tunnel tests normally provide the bulk of the derivative information, a limited in-flight verification of these data is required before proceeding to the more critical areas of the flight envelope.

In keeping with this general approach, the following three objectives may be listed for the current X-15 derivative program:

- (1) Establish progressively the basic in-flight stability and control

*This document is based on a paper presented at the Conference on the Progress of the X-15 Project, Edwards Air Force Base, Calif., November 20-21, 1961. Appendix B has been added to briefly describe the methods employed for determining the derivative characteristics from flight data.

**Title, Unclassified.



DECLASSIFIED BY AUTHORITY OF NASA
CLASSIFICATION CHANGE NOTICES NO. 14
DATED 4-21-65 ITEM NO. 6

H
2
3
7

trends and, thus, achieve the highest possible safety and realism in projecting each follow-on flight; (2) Confirm as many as possible of the original design considerations, including the wind-tunnel and theoretical studies leading to the present configuration; (3) Clarify and correct any troublesome flight control problems which, of course, are not entirely unexpected in a program of this nature. The present status of the program in fulfilling these basic objectives comprises the essential background of this paper. Supplementary information, including a description of the airplane, is given in references 1 and 2.

Symbols used in this paper are defined in appendix A.

PRINCIPAL AERODYNAMIC EFFECTS

Before discussing the derivative characteristics in detail, it is desirable to note several factors which were particularly problematical in the design stage before an acceptable configuration for the entire flight envelope was reached. These factors are related primarily to the strong shock fields that are generated at high angles of attack in the upper speed range, as illustrated in figure 1, and, therefore, are of immediate concern in the flight program. Particularly evident is the marked asymmetry in flow conditions between the upper and lower vertical tails as angle of attack is increased. This asymmetry has its source in the high dynamic-pressure field surrounding the ventral on the lower side, and the highly expanded flow over the dorsal on the upper side. The relative effectiveness of the two surfaces, as shown in the left-hand plot of figure 2, can be approximated, from two-dimensional relationships, by the ratio of the dynamic pressure times the lift-curve slope for the local shock flow to that for the free stream. The combination of high ventral effectiveness and low dorsal effectiveness noted at the higher angles of attack can be expected to generate some irregularity, as shown subsequently, in the effective dihedral and yaw control characteristics. The present tail configuration with approximately 45 percent of the total exposed area below the fuselage was selected as the best compromise for averting an excessive dihedral effect at low speeds while, at the same time, providing adequate directional stability during powered flight at high Mach numbers and altitudes. The adequacy of this arrangement for the entire flight envelope could, of course, be proven only under actual flight conditions.

The second effect, shown on the right in figure 2, is the rather diverse nature of the downwash at the horizontal tail. The results shown were estimated from two-dimensional shock-flow relationships and also originate in the high degree of asymmetry in flow conditions above and below the fuselage at high Mach numbers. The small upflow at low angles of attack, followed by an increasing downwash at the higher angles,


will lead to a nonlinear unstable trend in the longitudinal characteristics. This trend is further intensified as the leading edges of the horizontal tail at negative trim settings gradually penetrate the region of high dynamic pressure due to the wing compression shocks. Also, an increased pitch-control effectiveness will accompany the rise in dynamic pressure. Some evidence of these effects is shown subsequently, although little flight testing has been conducted under the conditions where these effects are most prevalent.

H
2
3
7
A third shock effect, shown in figure 3, is the gradual growth of a nonlinear trend in the lift-curve slope for the wing and tail surfaces as hypersonic speeds are approached. This trend, as shown in reference 2, can also be calculated from two-dimensional shock-flow relationships, and is such as to compensate for much of the stability loss due to the wing downwash and compression effects at high angles of attack. The nonlinearity first becomes significant at a Mach number of about 3 and changes relatively little at Mach numbers above 10. The slope at zero angle of attack in each case is equal to the familiar $4/\beta$ given by supersonic linear theory.

FLIGHT TESTS AND ANALYSIS

An overall survey of the areas in which flight measurements of the derivatives have been made is shown in figure 4. The angle-of-attack and Mach number coverage in relation to the overall flight envelope is indicated by the shaded region. Also included is an outer boundary (dashed line) representing the limits to which the airplane has actually been flown. Although the derivative coverage is uniformly shaded, the measurements are actually spotty in many areas and are limited largely to the static stability and control effectiveness. In particular, there is a scarcity of data at the higher Mach numbers and angles of attack where many of the basic problem areas lie. This, therefore, is the area on which much of the future X-15 program will be focused.

A somewhat simplified approach was taken in extracting the derivatives from the flight data. Approximate relationships based on measurements of the frequency, damping ratio, and certain amplitude ratios as shown in appendix B were found to be adequate for control-fixed dynamic responses. Where control inputs were also involved, an analog-matching technique was applied. These various methods are described more fully in reference 1. In general, the body-axes coordinate system has been employed throughout the analysis.



DISCUSSION

Longitudinal Characteristics

Static stability.- Three representative examples of the longitudinal static-stability characteristics as derived from gradual pull-up maneuvers are presented in figure 5. Shown are the angle-of-attack variations of normal-force coefficient and stabilizer incidence for approximately trimmed flight at a transonic, a supersonic, and a low hypersonic Mach number. The wind-tunnel data are also included (faired lines). In general, the trends of the data are as expected with increasing Mach number, and the flight and wind-tunnel results are in fairly good agreement. At the transonic Mach number, a nonlinear trend in the apparent stability, as shown by the stabilizer trim variation, was confirmed in flight. At the highest Mach number ($M = 5$) there is also an indication of the previously mentioned nonlinear trend in the lift-curve slope. A fair degree of stability is still evident for this Mach number, although some tendency toward reduced stability is observed in the upper angle-of-attack range. This effect is an example of the destabilizing influence of the downwash and dynamic pressure as angle of attack is increased at high Mach numbers.

The effect of Mach number on the lift and stability characteristics as determined from dynamic, or pulse-type, maneuvers is summarized in figure 6. The slope $C_{N\alpha}$ is given in the upper portion of the figure, and the stability derivative $\frac{dC_m}{dC_N}$, which is also a direct measure of the static margin in terms of the mean aerodynamic chord, is given in the lower plots. For the angle-of-attack ranges represented, good agreement is noted among the various data with the exception of the calculated stability in the high angle range. A discrepancy at Mach numbers above 3 is attributed to neglecting the nonlinear downwash and dynamic-pressure effects mentioned previously. The results indicate that, in general, the anticipated levels of stability have been realized in flight, at least in the regions of the envelope which have been covered.

Control.- Some typical results for the longitudinal control effectiveness are presented in figure 7. Again, in general, the results from wind-tunnel tests and theory agree fairly well with the flight data. The peak effectiveness occurs at a slightly lower Mach number than the peak stability shown in figure 6. The opposing trends in the intermediate Mach number range, one rising and the other diminishing, produce a noticeable transonic speed instability.

Figure 8 shows the trim characteristics for the maximum and two intermediate negative stabilizer settings. A potential trim capability

~~CONFIDENTIAL~~


approaching an angle of attack of 30° is noted at peak speeds, although, in general, very little flight data have been obtained in the high-angle range. The data that are available, however, seem to be generally in good agreement with the wind-tunnel predictions. The marked rise in trim capability above a Mach number of 3 again is caused by the nonlinear downwash and wing compression effects at high angles of attack.

H
2
3
7
Damping.- The last remaining derivative of interest for the longitudinal mode, the damping derivative, is summarized for a moderate angle-of-attack range in the left-hand plot of figure 9. This derivative is more difficult to isolate than the static derivatives, particularly in the supersonic range where the natural damping of the airplane is low. The flight and predicted results, however, are in fair agreement. The marked decline in the damping at supersonic speeds is indicated in the right-hand plot where the damping ratios corresponding to the various derivative points on the left are shown for a moderate dynamic pressure. The damping ratio drops well below 0.1 at Mach numbers above 2, and some form of damping augmentation must be provided.

Lateral-Directional Characteristics

Static stability.- As is often the case, the lateral-directional modes pose a greater variety of stability and control problems than the longitudinal modes. The two most important derivatives affecting the lateral-directional modes are the directional stability and dihedral effect shown in figure 10. Representative variations of the two derivatives with angle of attack as determined from both flight and wind-tunnel tests are presented for a low (1.9) and a high (4.0) supersonic Mach number. The flight data for $C_{n\beta}$ are low in some areas, but otherwise generally confirm the wind-tunnel predictions. The results show that, by distributing a large portion of the vertical-tail area below the fuselage, a relatively low dihedral effect has been achieved at the lower Mach number. The static directional stability $C_{n\beta}$, however, diminishes substantially with increasing angle of attack. At the higher Mach number the dihedral derivative, although still small, is of opposite sign. This unfavorable trend has a pronounced effect on the closed-loop dynamic stability, as discussed in reference 3. The cause for this positive trend is the previously mentioned asymmetry in effectiveness between the upper and lower vertical tails. As expected, the directional stability is lower at the higher Mach number but, because of the high intensity of the wing and bow compression shocks, increases rather than diminishes with increasing angle of attack.

The influence of the dihedral derivative on the Dutch roll stability for the two Mach numbers of 1.9 and 4.0 is illustrated in figure 11. The Dutch roll stability is represented by the parameter $(C_{n\beta})^*$ and



is given approximately by the relationship shown in the figure. (See references 4 and 5.) For comparison, the wind-tunnel values for $C_{n\beta}$ (dashed line) are carried over from the previous figure. It is especially important to note that the ratio of the moments of inertia about the yaw and roll axes in the second term of the equation is a large quantity (approximately 22), thus, the influence of the dihedral derivative is greatly magnified as angle of attack is increased. For the lower Mach number ($M = 1.9$), the dihedral derivative is negative, thereby augmenting the static stability. Conversely, for the higher Mach number ($M = 4.0$), the positive values of the dihedral derivative detract substantially from the basic stability. Similar effects are also found for the damping of the Dutch roll oscillation (eq. (32)).

One possible method of alleviating the adverse dihedral effect at the higher Mach numbers is to remove the lower rudder. This effect for a Mach number of 4.0 is shown in figure 12. The rudder-off configuration is represented by the dashed lines, which show that the sign of $C_{l\beta}$ has been reversed in a favorable direction, as desired. The directional stability $C_{n\beta}$, as anticipated, has also been markedly degraded, although much of the loss indicated can be regained by opening the speed brakes. The effect of the lower rudder on the Dutch roll stability $(C_{n\beta})^*$ is shown in the right-hand plot, where a considerable improvement due to the favorable dihedral effect is indicated at the higher angles of attack even though the speed brakes are closed. It should be mentioned that for Mach numbers less than about 2.2, the dihedral derivative is normally negative at all angles of attack, and the stability of the basic airplane is generally superior to that for the rudder-off configuration.

The directional stability and dihedral effect for the rudder-on configuration at low and moderate angles of attack are summarized in figures 13 and 14. Data are presented for both open and closed speed brakes, and corresponding results from wind-tunnel tests and theory are included. The results for the directional stability (fig. 13) indicate that the design levels have been essentially realized in flight, although the trend of the flight data is somewhat low at supersonic Mach numbers. There is also an apparent scatter in the flight increment for $C_{n\beta}$ due to speed-brake deflection in the lower angle-of-attack range. This is believed to be largely the result of differences in angle of attack within the 2° to 6° range, although the wind-tunnel data for this increment show relatively little sensitivity to angle of attack. The flight data for the dihedral derivative in figure 14 generally appear to confirm the wind-tunnel measurements for both angle-of-attack ranges. The speed-brake effect for this derivative is relatively small and is within the scatter of the data. Although the

theory from reference 2 predicts a positive trend in $C_{l\beta}$ at Mach numbers above 2, the prediction is excessively high at Mach numbers greater than 4. The source of the discrepancy is believed to be the assumption of two-dimensional shock compression and expansion flows in the vicinity of the vertical tails, whereas the actual shock effects stem largely from the bow wave and, therefore, are somewhat less severe. In general, comparisons similar to those shown in figure 14 have been obtained for angles of attack as high as 16° for the basic airplane and 9° for the rudder-off configuration.


Control. - As would be expected, most of the various effects due to shock interaction and removal of lower rudder are also reflected in the control characteristics for the lateral-directional modes. Typical results for the basic airplane at the two representative Mach numbers of 1.9 and 4.0 are given in figures 15 and 16. The roll and yaw effectiveness $C_{l\delta_a}$ and $C_{n\delta_v}$ as well as the cross-coupling

derivatives $C_{n\delta_a}$ and $C_{l\delta_v}$ are plotted against angle of attack, and

a comparison is made between the flight and wind-tunnel data. The effectiveness derivatives $C_{l\delta_a}$ and $C_{n\delta_v}$ are relatively insensitive

to angle of attack and, as expected, diminish with increasing Mach number. The yaw due to roll control is a relatively small quantity and remains positive (or favorable) throughout the flight envelope. The coupling effect in this case arises largely from the negative dihedral in the horizontal tail and the pressure gradient induced over the rear end of the fuselage. The roll due to yaw control not only varies with angle of attack, but also differs markedly between the two Mach numbers. The negative trend for the higher Mach number is due to the asymmetry in effectiveness between the upper and lower rudders at high angles of attack and would pose some difficulty in controlling the airplane if the rudders were used under these conditions, particularly because of the low moment of inertia about the roll axis. An interconnect between the yaw and roll channels is provided to correct this undesirable effect when the damping augmentation system is engaged. With the lower rudder removed, the yaw control effectiveness is much lower than before, but the roll due to yaw control does not reverse sign at the higher Mach numbers. The loss in effectiveness has not noticeably compromised the overall controllability of the airplane, however.

Figure 17 summarizes the influence of Mach number on the control derivatives for a low angle-of-attack range. Except in one area, the flight and wind-tunnel trends generally agree. The exception is the low trend of the flight data for the yaw control effectiveness at Mach numbers above 2. This discrepancy is of uncertain origin and appears to coincide approximately with the reduced directional stability noted



previously. Theory as derived from reference 2 overestimates both the yaw control effectiveness and roll due to yaw control at Mach numbers above 4. The discrepancies are believed to be due to the use of purely two-dimensional shock-flow relationships for estimating the vertical-tail effectiveness, whereas the actual flows are more nearly three-dimensional, as mentioned previously.

Damping. - The damping trends for the lateral-directional mode are much the same as those for the longitudinal mode considered previously. It suffices, therefore, to point out that the lateral-directional damping also decays to very low levels at supersonic speeds and that damping augmentation must be provided.


CONCLUDING REMARKS

The X-15 flight program has established fairly well defined derivative trends for Mach numbers approaching the design limit. With few exceptions, these trends have agreed well with the wind-tunnel predictions. Also, many of the basic stability and control design parameters have been confirmed in a substantial portion of the overall flight envelope. The gradual development of these basic trends from one flight to the next has, in fact, generated a high level of confidence in proceeding to more critical flight areas. No serious flight control problems have been encountered in the longitudinal mode; however, one serious deficiency in the lateral-directional mode has been observed in the form of an adverse dihedral effect at high Mach numbers and angles of attack. Further studies and tests are planned for the high Mach number and angle-of-attack ranges to reveal any further flight control problems that may exist in these more critical areas and to fill out the remainder of the flight envelope.

Flight Research Center

National Aeronautics and Space Administration

Edwards, Calif., November 20, 1961



APPENDIX A

SYMBOLS

In the following list of symbols, all angles are measured in radians, except as noted, and all coefficients are based on a body axis system with the longitudinal axis coinciding with the fuselage center-line.

b wing span, ft

C_l rolling-moment coefficient, $\frac{\text{Rolling moment}}{\bar{q}Sb}$

$$C_{l_p} = \frac{\partial C_l}{\partial \left(\frac{pb}{2V} \right)}$$

$$C_{l_r} = \frac{\partial C_l}{\partial \left(\frac{rb}{2V} \right)}$$

$$C_{l_\beta} = \frac{\partial C_l}{\partial \beta}$$

$$C_{l_{\delta_a}} = \frac{\partial C_l}{\partial \delta_a}$$

$$C_{l_{\delta_v}} = \frac{\partial C_l}{\partial \delta_v}$$

C_m pitching-moment coefficient, $\frac{\text{Pitching moment}}{\bar{q}S\bar{c}}$

$$C_{m_q} = \frac{\partial C_m}{\partial \left(\frac{q\bar{c}}{2V} \right)}$$

$$C_{m_\alpha} = \frac{\partial C_m}{\partial \alpha}$$

$$C_{m\dot{\alpha}} = \frac{\partial C_m}{\partial \left(\frac{\dot{\alpha} \bar{c}}{2V} \right)}$$

$$C_{m\delta_h} = \frac{\partial C_m}{\partial \delta_h}$$

$$C_N \quad \text{normal-force coefficient, } \frac{\text{Normal force}}{\bar{q}S}$$

$$C_{N\alpha} = \frac{\partial C_N}{\partial \alpha}$$

$$C_{N\delta_h} = \frac{\partial C_N}{\partial \delta_h}$$

$$C_n \quad \text{yawing-moment coefficient, } \frac{\text{Yawing moment}}{\bar{q}Sb}$$

$$C_{n_p} = \frac{\partial C_n}{\partial \left(\frac{pb}{2V} \right)}$$

$$C_{n_r} = \frac{\partial C_n}{\partial \left(\frac{rb}{2V} \right)}$$

$$C_{n\beta} = \frac{\partial C_n}{\partial \beta}$$

$$\left(C_{n\beta} \right)^* = C_{n\beta} - \alpha \frac{I_Z}{I_X} C_{l\beta}$$

$$C_{n\delta_a} = \frac{\partial C_n}{\partial \delta_a}$$

H
2
3
7

$$c_{n\delta_v} = \frac{\partial c_n}{\partial \delta_v}$$

$$C_Y \quad \text{side-force coefficient, } \frac{\text{Side force}}{\bar{q}S}$$

$$C_{Y\beta} = \frac{\partial C_Y}{\partial \beta}$$

$$\bar{c} \quad \text{mean aerodynamic chord, ft}$$

$$c_n \quad \text{normal-force coefficient for two-dimensional flat plate}$$

$$I_X \quad \text{moment of inertia about longitudinal axis, slug-ft}^2$$

$$I_Y \quad \text{moment of inertia about lateral axis, slug-ft}^2$$

$$I_Z \quad \text{moment of inertia about vertical axis, slug-ft}^2$$

$$L_p = \frac{\bar{q}Sb^2C_{l_p}}{2VI_X}$$

$$L_r = \frac{\bar{q}Sb^2C_{l_r}}{2VI_X}$$

$$L_\beta = \frac{\bar{q}SbC_{l_\beta}}{I_X}$$

$$L_{\delta_a} = \frac{\bar{q}SbC_{l_{\delta_a}}}{I_X}$$

$$L_{\delta_v} = \frac{\bar{q}SbC_{l_{\delta_v}}}{I_X}$$

$$M \quad \text{Mach number}$$

$$M_q = \frac{\bar{q}S\bar{c}^2C_{m_q}}{2VI_Y}$$

H
2
3
7



$$M_{\alpha} = \frac{\bar{q} S \bar{c} C_{m_{\alpha}}}{I_Y}$$

$$M_{\delta_h} = \frac{\bar{q} S \bar{c} C_{m_{\delta_h}}}{I_Y}$$

m airplane mass, slugs

$$N_p = \frac{\bar{q} S b^2 C_{n_p}}{2 V I_Z}$$

$$N_r = \frac{\bar{q} S b^2 C_{n_r}}{2 V I_Z}$$

$$N_{\beta} = \frac{\bar{q} S b C_{n_{\beta}}}{I_Z}$$

$$N_{\delta_a} = \frac{\bar{q} S b C_{n_{\delta_a}}}{I_Z}$$

$$N_{\delta_v} = \frac{\bar{q} S b C_{n_{\delta_v}}}{I_Z}$$

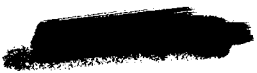
$$P = \frac{|p|}{|\beta|}$$

p rate of roll

$$\dot{p} = \frac{dp}{dt}$$

$$Q = \frac{|q|}{|\Delta \alpha|}$$

q pitching rate



$$\dot{q} = \frac{dq}{dt}$$

\bar{q} free-stream dynamic pressure, lb/sq ft

$$R = \frac{|r|}{|\beta|}$$

r rate of yaw

$$\dot{r} = \frac{dr}{dt}$$

S reference area equal to area of wing with leading and trailing edges extended to plane of symmetry

t time, sec

V free-stream velocity, ft/sec

$$Y_{\beta} = \frac{\bar{q}SC_{Y\beta}}{mV}$$

$$Z_{\alpha} = \frac{\bar{q}SC_{N\alpha}}{mV}$$

$$Z_{\delta_h} = \frac{\bar{q}SC_{N\delta_h}}{mV}$$

α angle of attack

$\dot{\alpha}$ time rate of change of angle of attack due to constant vertical acceleration (plunging motion)

$\Delta\alpha$ increment in angle of attack as measured from that for trimmed steady-state flight

$\Delta\dot{\alpha}$ time rate of change of increment of angle of attack due to constant vertical acceleration (plunging motion)

β angle of sideslip

H
2
3
7

[REDACTED]

$\dot{\beta}$	time rate of change of sideslip angle due to constant lateral acceleration
γ	phase angle between vectors p and β
δ_a	differential incidence of horizontal-tail panels, positive for a downward deflection of the leading edge of right-hand panel relative to the left-hand panel
δ_h	incidence of horizontal tail measured in plane of symmetry relative to fuselage centerline, positive for upward rotation of leading edge
$\Delta\delta_h$	incremental change in incidence of the horizontal tail measured in plane of symmetry relative to fuselage centerline, positive for upward rotation of leading edge
δ_v	deflection angle of directional-control surfaces, positive for rotation of leading edge to right
ϵ	downwash angle, deg
ζ	ratio of natural damping to critical damping
μ	phase angle between vectors q and $\Delta\alpha$
ν	phase angle between vectors r and β
ϕ	angle of bank
ω	undamped natural frequency, radians per sec
ω_d	damped natural frequency, $\omega\sqrt{1 - \zeta^2}$, radians per sec
Subscript:	
l	local flow conditions

AT

APPENDIX B

Method for Determining the Derivatives From Flight Data

The following presentation is a somewhat generalized approach to the vector method currently employed in the X-15 derivative program. It is, therefore, supplementary to the more rigorous treatment given in reference 1 for the lateral-directional derivatives. Further details may also be found in references 6 and 7.

The method, in general, is predicated on the measurement in flight of time histories of the angular accelerations \dot{p} , \dot{q} , \dot{r} , velocities p , q , r , and displacements ϕ , α , β about the roll, pitch, and yaw axes, respectively, as well as the corresponding control-surface positions δ_a , δ_h , δ_v . It is further assumed that the airplane transients following an abrupt control input (pulse) are, simply, damped sinusoidal oscillations which may be represented in the vector form

$$A = |A|e^{-\zeta\omega t}e^{i\omega_d t}e^{i\sigma} \quad (1)$$

where A is the amplitude of a particular quantity, $\zeta\omega$ the damping coefficient, ω_d the damped natural frequency, and σ the phase angle measured from some convenient reference point.

The motions are assumed to be small and, since the product of inertia and the rotary derivatives L_r and N_p for the X-15 are small and negligible, the following linearized equations of motion based on a body-axes system are applicable:

Longitudinal

$$\Delta\dot{\alpha} = q + Z_\alpha\Delta\alpha + Z_{\delta_h}\Delta\delta_h \quad (2)$$

$$\dot{q} = M_q q + M_\alpha\Delta\alpha + M_{\delta_h}\Delta\delta_h \quad (3)$$

Lateral-directional

$$\dot{p} = L_\beta\beta + L_p p + L_{\delta_a}\delta_a + L_{\delta_v}\delta_v \quad (4)$$

$$\dot{r} = N_\beta\beta + N_r r + N_{\delta_a}\delta_a + N_{\delta_v}\delta_v \quad (5)$$

$$\dot{\beta} = Y_\beta\beta - r + \alpha p \quad (6)$$

In accordance with the previously stipulated assumptions, the following mode shapes and phase relationships are defined:

Longitudinal

$$\Delta\alpha = |\Delta\alpha|e^{-\zeta\omega t}e^{i\omega_d t} \quad \dot{\Delta\alpha} = (-\zeta\omega + i\omega_d)\Delta\alpha \quad (7)$$

$$q = |q|e^{-\zeta\omega t}e^{i\omega_d t}e^{i\mu} \quad \dot{q} = (-\zeta\omega + i\omega_d)q \quad (8)$$

where

μ is the phase angle between q and $\Delta\alpha$

Lateral-directional

$$\beta = |\beta|e^{-\zeta\omega t}e^{i\omega_d t} \quad \dot{\beta} = (-\zeta\omega + i\omega_d)\beta \quad (9)$$

$$p = |p|e^{-\zeta\omega t}e^{i\omega_d t}e^{i\gamma} \quad \dot{p} = (-\zeta\omega + i\omega_d)p \quad (10)$$

$$r = |r|e^{-\zeta\omega t}e^{i\omega_d t}e^{i\nu} \quad \dot{r} = (-\zeta\omega + i\omega_d)r \quad (11)$$

where

γ is phase angle between p and β

ν is phase angle between r and β

For control-fixed transient oscillations, the substitution of the above expressions (eqs. (7) to (11)) into equations (2) to (6) results in the following:

Longitudinal

$$(Z_\alpha + \zeta\omega + Q \cos \mu) + i(-\omega_d + Q \sin \mu) = 0 \quad (12)$$

$$(M_\alpha + Q\zeta\omega \cos \mu + Q\omega_d \sin \mu + QM_q \cos \mu) + i(-Q\omega_d \cos \mu + Q\zeta\omega \sin \mu + QM_q \sin \mu) = 0 \quad (13)$$

where

$$Q = \frac{|q|}{|\Delta\alpha|}$$

CONFIDENTIAL

Lateral-directional

$$\left(\frac{L_\beta}{P} + \zeta\omega \cos \gamma + \omega_d \sin \gamma + L_p \cos \gamma \right) + i(-\omega_d \cos \gamma + \zeta\omega \sin \gamma + L_p \sin \gamma) = 0 \quad (14)$$

$$\left(\frac{N_\beta}{R} + \zeta\omega \cos \nu + \omega_d \sin \nu + N_r \cos \nu \right) + i(-\omega_d \cos \nu + \zeta\omega \sin \nu + N_r \sin \nu) = 0 \quad (15)$$

$$\left(Y_\beta + \zeta\omega - R \cos \nu + \alpha P \cos \gamma \right) + i(-\omega_d - R \sin \nu + \alpha P \sin \gamma) = 0 \quad (16)$$

where

$$P = \frac{|p|}{|\beta|} \quad R = \frac{|r|}{|\beta|}$$

The two parts in each expression represent mutually perpendicular vector components of the motion, and, therefore, must sum to zero independently. Four independent relationships are thus available for the longitudinal mode and six for the lateral-directional mode.

Longitudinal Derivatives

The imaginary part of equation (13) gives

$$\tan \mu = \frac{\omega_d}{\zeta\omega + M_d} \quad (17)$$

It is generally found for the X-15 that $|\zeta\omega + M_d| \ll \omega_d$ and that $\mu \rightarrow \pi/2$. It then follows from equations (12) and (13) that

$$\omega_d = Q = \frac{|q|}{|\Delta\alpha|} \quad \text{and}$$



CONFIDENTIAL

$$Z_{\alpha} = -\zeta\omega \quad (18)$$

$$M_q = -\zeta\omega \quad (19)$$

$$M_{\alpha} = -\omega_d^2 = -\left(\frac{|q|}{|\Delta\alpha|}\right)^2 \quad (20)$$

Since the terms $\zeta\omega$, ω_d , and Q are readily obtainable from the flight data, the derivatives $C_{N_{\alpha}}$, C_{m_q} , and $C_{m_{\alpha}}$ are easily determined from the above relationships.

The control derivatives $C_{N_{\delta_h}}$ and $C_{m_{\delta_h}}$ are obtained directly from equations (2) and (3) and the accelerations initially developed during the pulses, as explained in references 1 and 7. Corrections for any small excursions in $\Delta\alpha$ and q that may occur are estimated from available or estimated values for Z_{α} , M_q , and M_{α} .

Lateral-Directional Derivatives

The phase angle ν between r and β as derived from the imaginary part of equation (15) is

$$\tan \nu = \frac{\omega_d}{\zeta\omega + N_r} \quad (21)$$

As in the case of μ (eq. (17)), $|\zeta\omega + N_r| \ll \omega_d$ and $\nu \rightarrow -\pi/2$. Equation (15) then gives immediately

$$N_r = -\zeta\omega \quad (22)$$

$$N_{\beta} = R\omega_d = \frac{|r|}{|\beta|} \omega_d \quad (23)$$

and, thus, the derivatives C_{n_r} and $C_{n_{\beta}}$ are readily obtained.

CONFIDENTIAL

The real and imaginary parts of equation (14) combine to give

$$\frac{L_\beta}{P} + \frac{\sin \gamma}{\omega_d} \left[\left(\zeta \omega + L_p \right)^2 + \omega_d^2 \right] = 0 \quad (24)$$

Using the imaginary part of equation (16) for $\sin \gamma$ gives

$$\frac{L_\beta}{P} + \frac{(\omega_d - R)}{\omega_d \alpha P} \left[\left(\zeta \omega + L_p \right)^2 + \omega_d^2 \right] = 0 \quad (25)$$

Noting that $\left(\zeta \omega + L_p \right)^2 \ll \omega_d^2$ and may be neglected,

$$L_\beta = \frac{\omega_d}{\alpha} \left(\frac{|r|}{|\beta|} - \omega_d \right) \quad (26)$$

from which C_{L_β} may be determined.

The derivatives L_p and Y_β are usually more difficult to isolate than N_r or the static derivatives, but may be approximated from equations (14) and (16) as follows:

$$Y_\beta = -\zeta \omega - \alpha \frac{|p|}{|\beta|} \cos \gamma \quad (27)$$

$$L_p = -\zeta \omega + \frac{\omega_d}{\tan \gamma} \quad (28)$$

where

$$\gamma = \sin^{-1} \left(\frac{\omega_d - \frac{|r|}{|\beta|}}{\alpha \frac{|p|}{|\beta|}} \right) \quad (29)$$

As $\alpha \rightarrow 0$, L_β can best be approximated by equations (24) and (28) giving

$$L_\beta = - \frac{|p|}{|\beta|} \frac{\omega_d}{\sin \gamma} \quad (30)$$

[REDACTED]

The control derivatives are obtained directly from the equations of motion (eqs. (4) and (5)) as discussed for the longitudinal mode.

The following inverse relationships may also be derived from the foregoing relationships:

$$\omega_d^2 \approx N_\beta - \alpha L_\beta \quad (31)$$

$$\zeta\omega \approx \frac{-Y_\beta N_\beta + \alpha L_\beta (L_p + Y_\beta)}{N_\beta - 2\alpha L_\beta} \quad (32)$$

$$\frac{|p|}{|\beta|} = \frac{-L_\beta}{\sqrt{N_\beta - \alpha L_\beta}} \quad \text{or} \quad \frac{|\phi|}{|\beta|} = \frac{-L_\beta}{N_\beta - \alpha L_\beta} \quad (33)$$

$$\cos \gamma \approx \frac{\zeta\omega + L_p}{\sqrt{N_\beta - \alpha L_\beta}} \quad (34)$$

$$\frac{|r|}{|\beta|} \approx \frac{N_\beta}{\sqrt{N_\beta - \alpha L_\beta}} \quad (35)$$

General Remarks

Where damping augmentation is provided through the control surfaces, the techniques described in the preceding sections can be conveniently employed for isolating the damper effects assuming that the damper-response characteristics and the control effectiveness are known.

Where irregular pilot-control inputs occur following the initial disturbance, the relationships derived in this appendix do not apply. In such instances, recourse is generally made to the analog-matching technique described in reference 1.

December 29, 1961.

AL

REFERENCES

1. Yancey, Roxanah B., Rediess, Herman A., and Robinson, Glenn H.: Aerodynamic-Derivative Characteristics of the X-15 Research Airplane as Determined From Flight Tests for Mach Numbers From 0.6 to 3.4. NASA TN D-1060, 1961.
2. Walker, Harold J., and Wolowicz, Chester H.: Theoretical Stability Derivatives for the X-15 Research Airplane at Supersonic and Hypersonic Speeds Including a Comparison With Wind-Tunnel Results. NASA TM X-287, 1960.
3. Petersen, Forrest S., Rediess, Herman A., and Weil Joseph: Lateral-Directional Control Characteristics of the X-15 Airplane. NASA TM X-726, 1962.
4. Moul, Martin T., and Paulson, John W.: Dynamic Lateral Behavior of High-Performance Aircraft. NACA RM L58E16, 1958.
5. Taylor, Lawrence W., Jr.: Analysis of a Pilot-Airplane Lateral Instability Experienced With the X-15 Airplane. NASA TN D-1059, 1961.
6. Etkin, Bernard: Dynamics of Flight. John Wiley & Sons, Inc., c. 1959.
7. Wolowicz, Chester H., and Holleman, Euclid C.: Stability-Derivative Determination From Flight Data. AGARD Rep. 224, 1958.

H
2
3
7

CONFIDENTIAL

PRINCIPAL FLOW PATTERNS

M=6

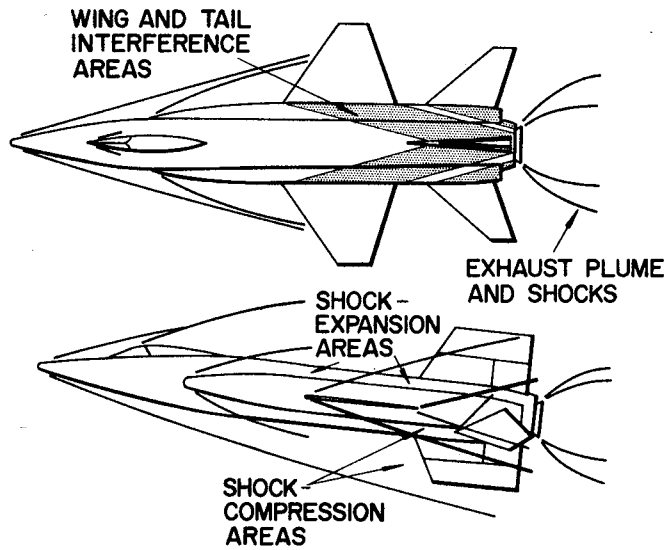


Figure 1

PROMINENT SHOCK-FLOW EFFECTS

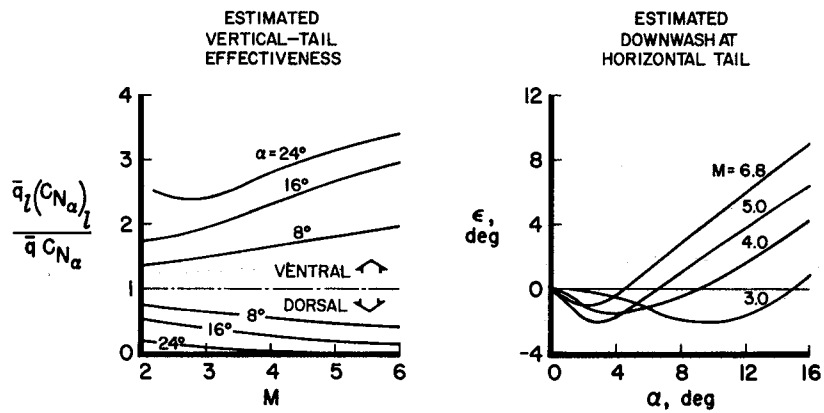


Figure 2

CONFIDENTIAL

TWO-DIMENSIONAL LIFT CHARACTERISTICS AT SUPERSONIC AND HYPERSONIC SPEEDS

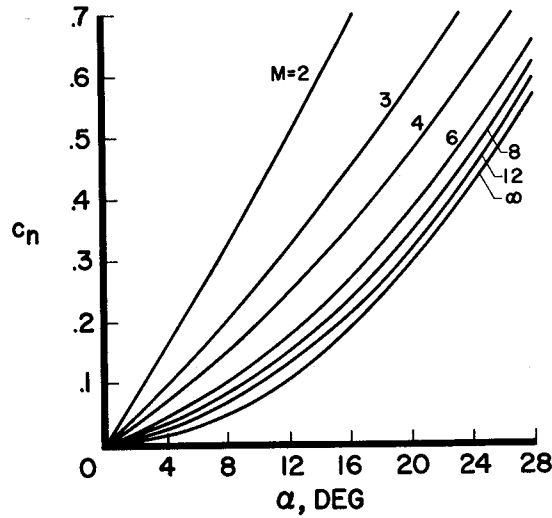


Figure 3

FLIGHT COVERAGE

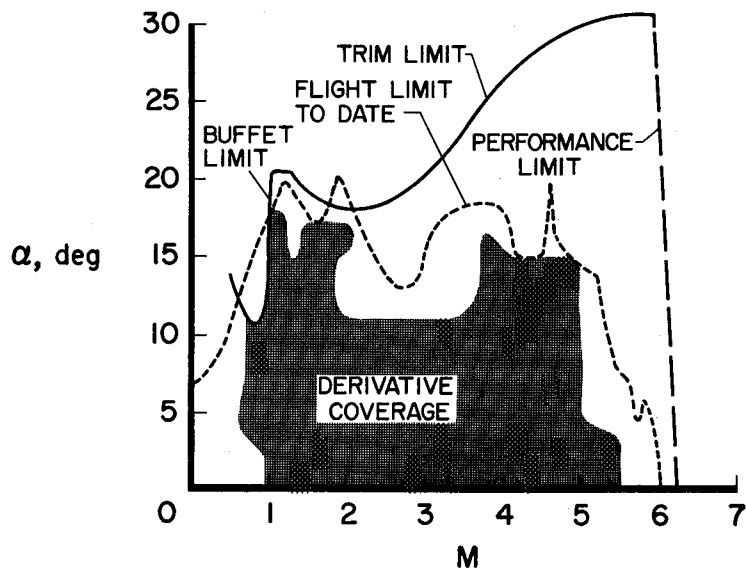


Figure 4

CONFIDENTIAL

LONGITUDINAL STATIC STABILITY

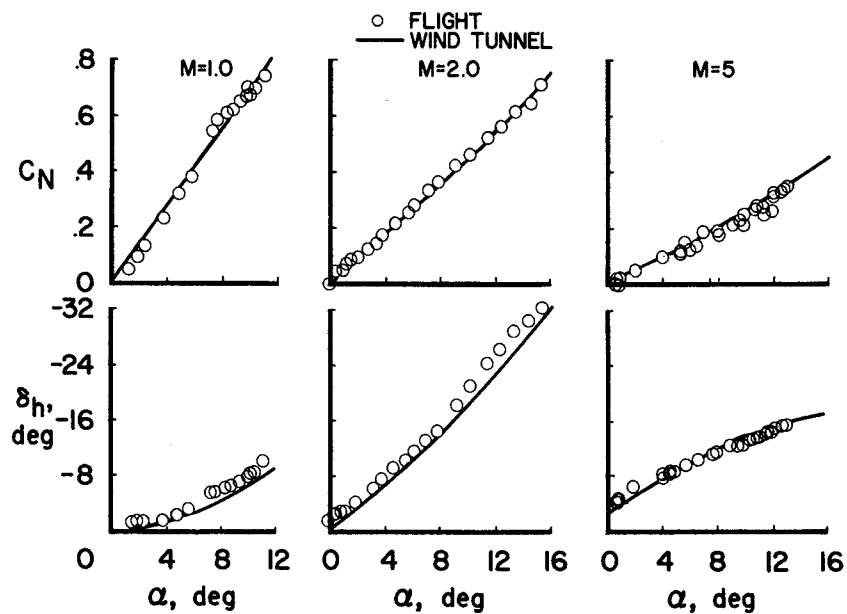


Figure 5

SUMMARY OF LONGITUDINAL STABILITY

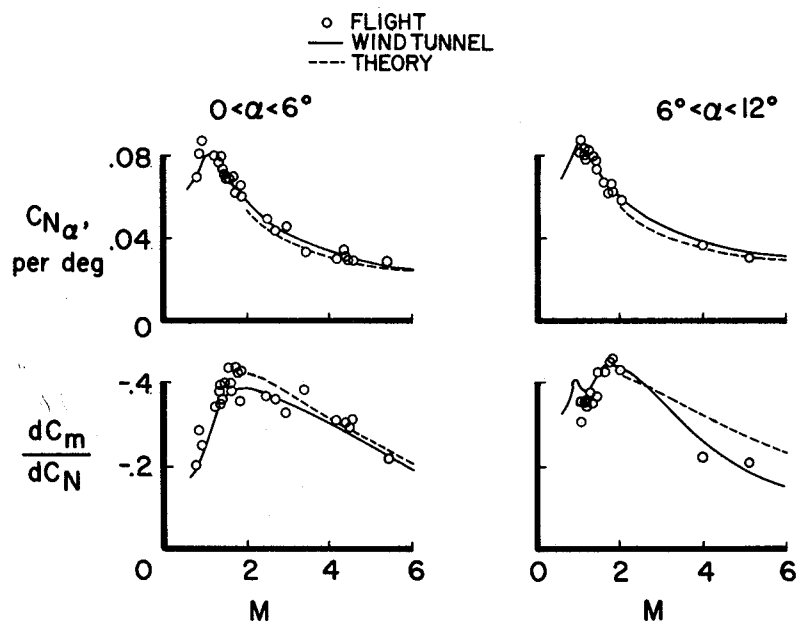


Figure 6

LONGITUDINAL CONTROL EFFECTIVENESS

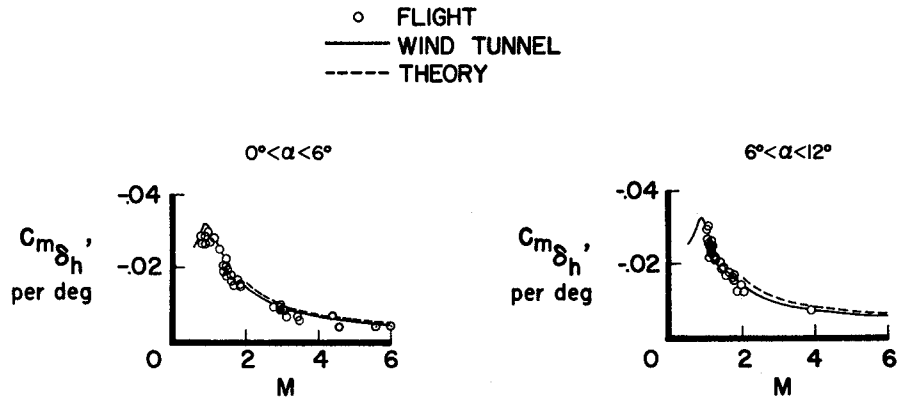


Figure 7

TRIM CAPABILITY

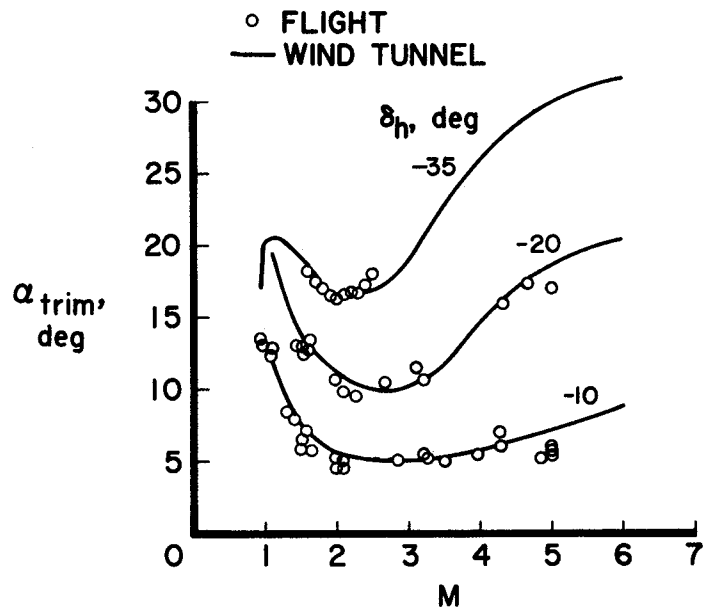


Figure 8

CONFIDENTIAL

LONGITUDINAL DAMPING

$$0^\circ < \alpha < 6^\circ$$

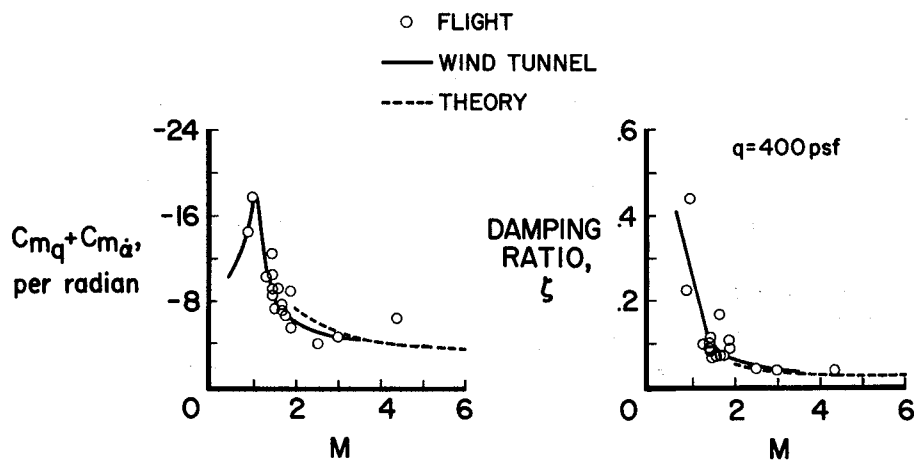


Figure 9

LATERAL-DIRECTIONAL STABILITY

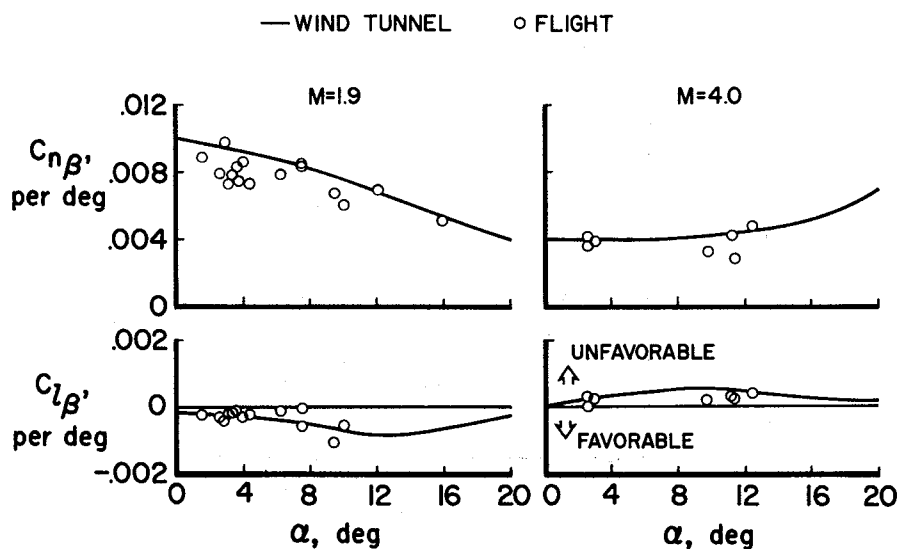


Figure 10

CONFIDENTIAL

27

DUTCH-ROLL STABILITY

$$(C_{n\beta})^* = C_{n\beta} - \alpha \frac{I_z}{I_x} C_{l\beta} \approx \frac{\omega^2}{qSb/l_z}$$

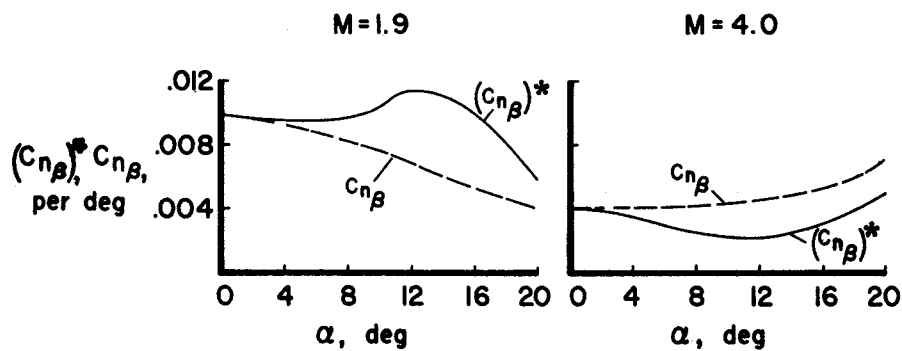


Figure 11

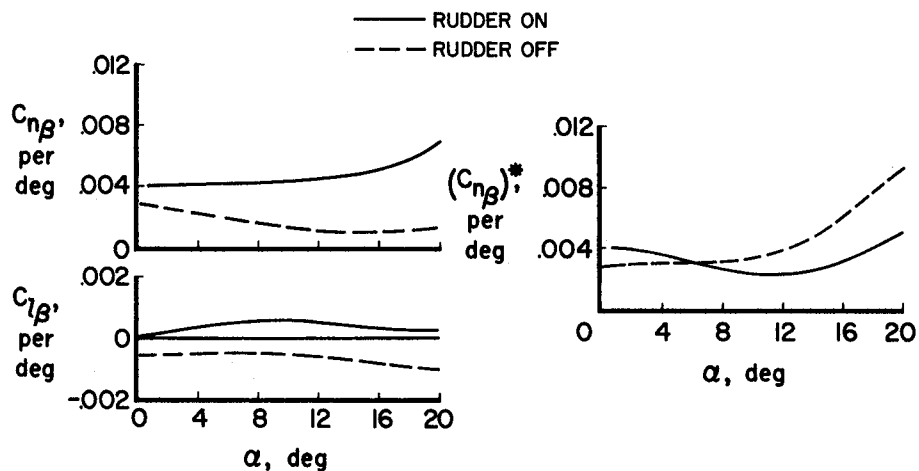
EFFECT OF LOWER RUDDER ON
LATERAL-DIRECTIONAL STABILITY
SPEED BRAKES CLOSED $M = 4.0$ 

Figure 12

CONFIDENTIAL

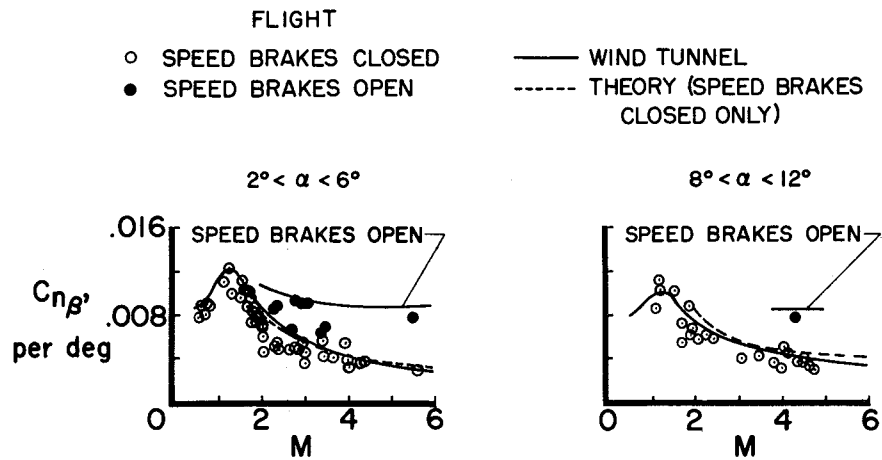
 $C_{n\beta}$ SUMMARY

Figure 13

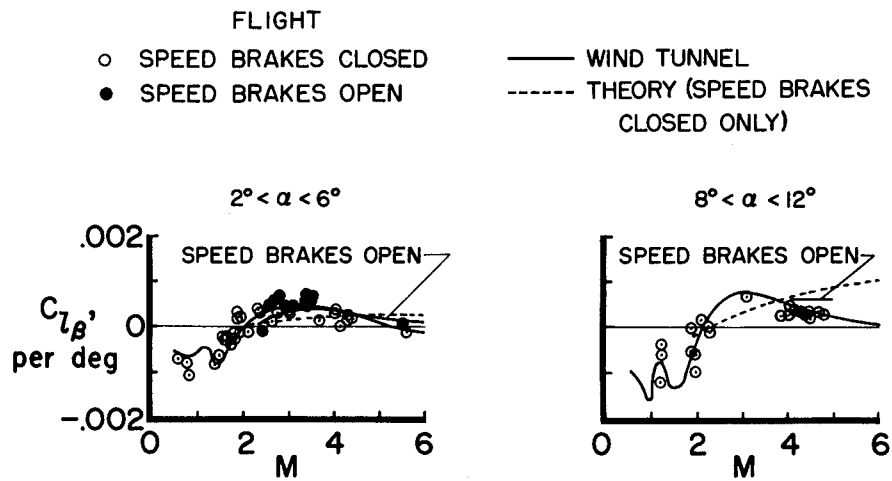
 $C_{l\beta}$ SUMMARY

Figure 14

H-237

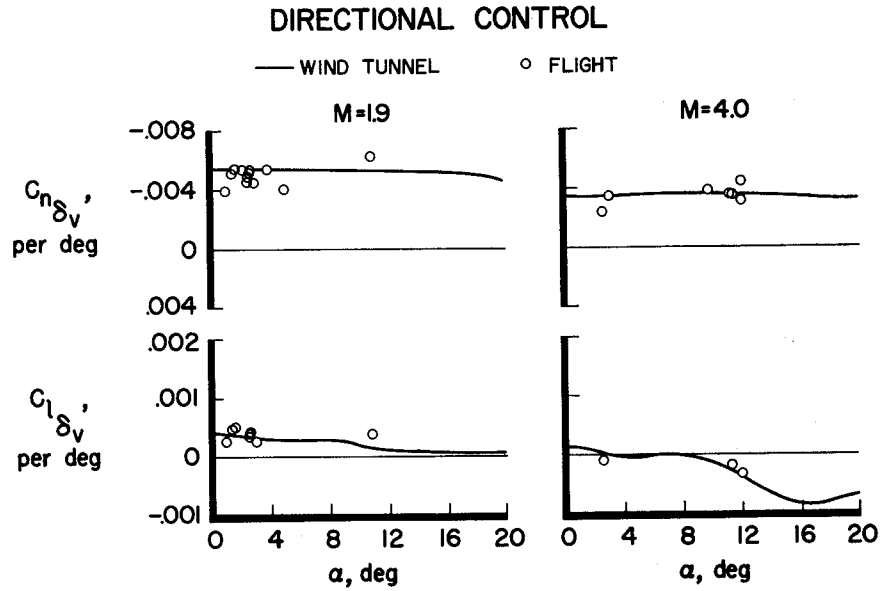


Figure 15

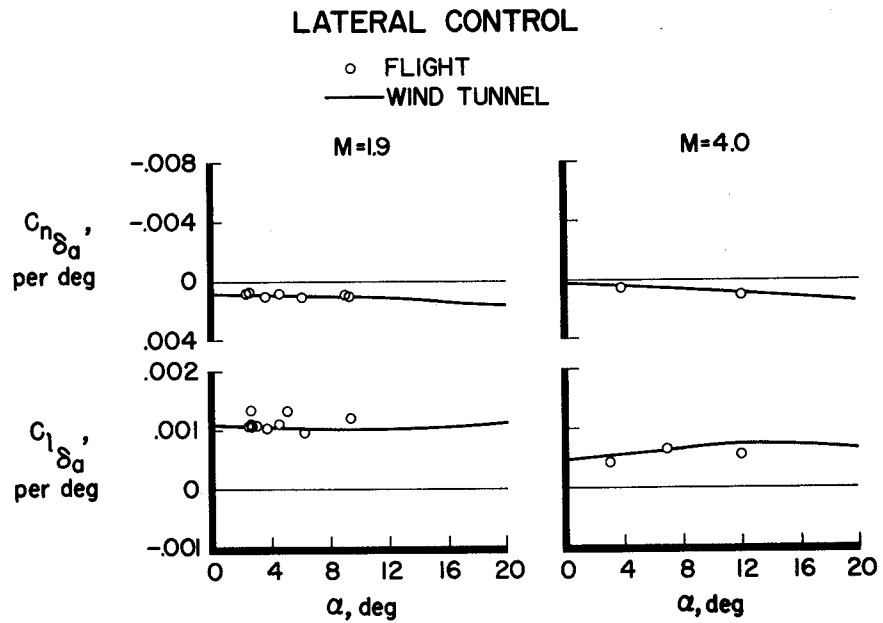


Figure 16



SUMMARY OF LATERAL-DIRECTIONAL CONTROL

$$0^\circ < \alpha < 5^\circ$$

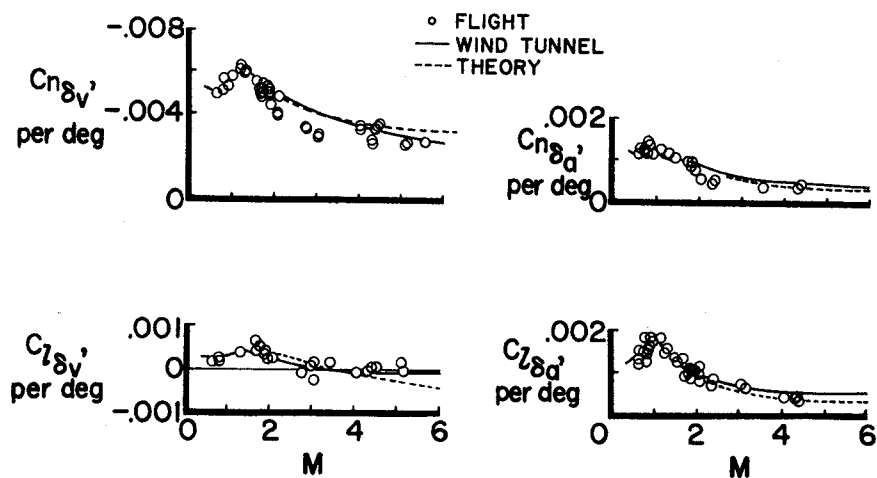


Figure 17